Role of Scaffold Architecture and Excess Surface Polymer Layers in a Three-Dimensionally Interconnected Ceramic/Polymer Composite Electrolyte

Ritu Sahore[1,*], Beth L. Armstrong[2], Xiaomin Tang[1], Changhao Liu[1], Kyra Owensby[3], Sergiy Kalnaus[4], Xi Chelsea Chen[1,*]

[1]*Oak Ridge National Laboratory, Chemical Sciences Division, Oak Ridge, Tennessee 37831, United States*
[2]*Oak Ridge National Laboratory, Materials Science and Technology Division, Oak Ridge, Tennessee 37831, United States*
[3]*The Bredesen Center for Interdisciplinary Research and Graduate Education, The University of Tennessee Knoxville, Knoxville, Tennessee 37996, United States*
[4]*Oak Ridge National Laboratory, Computational Science and Engineering Division, Oak Ridge, Tennessee 37831, United States*

Ritu Sahore (ORCID: 0000-0002-2390-9570): sahorer@ornl.gov
Beth L. Armstrong (ORCID: 0000-0001-7149-3576): armstrongbl@ornl.gov
Xiaomin Tang (ORCID: 0000-0002-0448-7261): mindytang66@gmail.com
Changhao Liu (ORCID: 0000-0002-9103-8834): chliu@udel.edu
Sergiy Kalnaus (ORCID: 0000-0002-7465-3034): kalnauss@ornl.gov
Xi Chelsea Chen (ORCID: 0000-0003-1188-7658): chenx@ornl.gov

*Corresponding authors.

Data Availability Statement

The data that support the findings of this study are available from the corresponding author upon request.

Conflict of Interest

The authors declare no conflict of interest.

Keywords: solid-state batteries, composite electrolyte, interconnected ceramic, polymer/ceramic interface, polymer electrolyte, ceramic electrolyte, interfaces, lithium

Abstract

Three-dimensionally interconnected ceramic/polymer composite electrolytes offer promise to combine the benefits of both ceramic and polymer electrolytes. However, an in-depth understanding of the role of ceramic scaffold's architecture, and the associated polymer/ceramic interfaces on the electrochemical properties of such composite electrolytes is still incomplete. Here, these factors are systematically evaluated using an interconnected composite electrolyte with

a tunable and well-defined architecture. The ionic conductivity of the ceramic scaffold is strongly dependent on its porosity and tortuosity, as demonstrated experimentally and via theoretical modeling. The connectivity of the ceramic framework avoids the high interfacial impedance at the polymer/ceramic electrolyte interface within the composite. However, this work discovers that the interfacial impedance between the bulk composite and excess surface polymer layers of the composite membrane dominates the overall impedance, resulting in a one to two orders drop of ionic conductivity compared to the ceramic scaffold. Despite the high impedance interfaces, an improved Li^+ transference number is found compared to the neat polymer (0.29 vs. 0.05), attributed to the ceramic phase's contributions towards ion transport. This leads to flatter overpotentials in lithium symmetric cell cycling. These results will guide future research directions towards scalable manufacturing of composite electrolytes with optimized architecture and interfaces.

Introduction

To achieve the high-energy densities promised by solid-state batteries, a thin separator electrolyte layer will be required that can, at a minimum, sustain high current densities (>4 mA/cm^2) without causing significant voltage-drop across it, suppress lithium dendrite propagation, and is easily processible.[1, 2] Dense 100% ceramic electrolyte layers can theoretically fulfil these requirements due to their high room temperature (RT) ionic conductivity, Li^+ transference number of one, and high modulus.[3] However, good processibility and fracture toughness of such layers is a challenge.[3] Incorporation of polymer electrolytes to ceramic, a.k.a. composite polymer electrolytes (CPEs), can impart flexibility and toughness to this layer, and improve processibility.[4] However, it has been shown for several polymer-ceramic combinations that the classic CPE design of ceramic particles dispersed within a polymer matrix does not utilize the high ionic conductivity of the ceramic despite exceeding the percolation threshold, because of the high interfacial impedance (several $k\Omega\text{-}cm^2$ at 20 ºC) of the polymer/ceramic interface at RT.[5-11] This leads to unsatisfactorily low ionic conductivity of the composite membrane at RT. Plasticizing has been shown to help reduce the interfacial impedance dramatically.[5] Although, in a practical solid state battery with a thin lithium metal anode, the plasticizer can be detrimental in quickly consuming the limited lithium metal reservoir.[12]

In order to overcome this issue, another design consisting of a 3-dimensionally interconnected ceramic has been reported previously by our group and others.[13-20] The interconnectedness of the ceramic allows lithium ion conduction to occur primarily through the ceramic phase while avoiding the high impedance polymer/ceramic interface. As one of the firsts, Fu et al. demonstrated a 3D-interconnected CPE by utilizing electrospinning to obtain a porous 3D-interconnected LLZO nanofibers mat which was infiltrated with linear poly(ethylene oxide) (PEO) based polymer electrolyte.[16] Zhai et al. later utilized freeze-tape casting to obtain a vertically-aligned 3D interconnected LATP-based porous network which was infiltrated with linear-PEO to obtain a 3D-interconnected CPE.[18] Several other strategies have been reported later on to obtain the 3D-interconnected ceramic backbones such as partial sintering (enough sintering to form particle-particle necks but not complete densification) of ceramic particles with or without the presence of sacrificial pore formers, partial sintering of sol-gel derived hydrogels, or utilization of porous templates.[13-15] Ionic conductivities of up to 2.5×10^{-4} S/cm at RT have been reported of these composite electrolytes, significantly improved compared to that of the linear-PEO-based polymer electrolyte (10^{-6}-10^{-7} S/cm at RT).[16] The enhancement in ionic-conductivity is ascribed mainly to generation of continuous, long-transport pathways for lithium-ions in not only the

interconnected ceramic phase but also the generation of a 3D-percolated highly conductive polymer/ceramic interphase layer.[14-16, 19-21]

Although a variety of ceramic electrolyte backbones have been utilized, there lacks a clear understanding of the role of its architecture i.e. porosity (specific surface area, specific pore volume) and tortuosity, on the resulting Li-ion transport properties of the backbone as well as the resulting composite. In some of the above-mentioned examples, the improvement in ionic conductivity is ascribed to fast ion-transport along both the continuous ceramic and polymer/ceramic interfacial phase, with the RT resulting ionic conductivities widely ranging from 6.8×10^{-6} to 2.5×10^{-4} S/cm. In another case, even without the use of an ionically conductive scaffold, ionic conductivity of 5.8×10^{-4} S/cm at RT was achieved, relying solely on the ceramic/polymer interfacial layer's high conductivity.[21] Hence, a more systematic understanding is needed to resolve the importance of these variables. In addition, in the above-described design for a composite membrane, presence of a pure polymer electrolyte layer on the surface can help achieve conformal contact with the two electrodes (anode, cathode) because of its soft and pliable nature compared to the ceramic.[22] Indeed, in majority of the above-mentioned references, a thin excess polymer layer is always present either as a deliberate design or as an indirect consequence of the infiltration process. However, the resistive polymer/ceramic interface that is avoided by the 3D-interconnected design now gets introduced at the two surfaces of the membrane, which was shown to significantly hamper the overall ionic conductivity of the membrane, especially for thin CPE membranes.[13] Curiously, this was never addressed nor did it seem to be an issue in the above-cited references on interconnected-composites given the high ionic conductivity of the resulting composites, given that majority of them did not use any plasticizer.

In this work, we utilize a tunable platform of partial sintering of ceramic electrolyte (LICGC™, $Li1_{+x+y}Al_xTi_{2-x}Si_yP_{3-y}O_{12}$) particles to prepare ionically conducting, randomly-interconnected scaffolds of varying porosities to understand the role of scaffold architecture on the transport properties of both the scaffold and the corresponding composite electrolytes (**Figure 1**). [13] We also study the effect of excess surface polymer layers in the CPEs of this design. We show that the porosity and tortuosity of the ceramic scaffold significantly impacted its ionic conductivity. At a porosity of around 50%, the conductivity of the scaffold is very sensitive to the volume fraction of voids and varies between 1-10% (an order of difference) of that of the dense ceramic plate. Theoretical modeling strongly suggests the role of tortuosity towards this observation. Polymer/ceramic composites were prepared with ceramic scaffolds of three different porosities: 0% (dense LICGC™ plate), 48 %, and 52 %. The porous scaffolds were first infiltrated with thermally curable polymer electrolyte precursors to form cross-linked PEO+LiTFSI – filled LICGC™ scaffold composites. Thin (<5 μm) linear PEO interlayers with controlled thickness were additionally applied to these composite electrolytes' two surfaces to act as protection layer between the lithium electrode and LATP-based ceramic (**Scheme 1**) and improve contact with the electrodes. The thin polymer layers also act as a proxy for excess polymer at the surface as a result of infiltration. These samples are referred to as "Trilayer CPEs" in the later text. Depending on the ceramic scaffold type, a drop in the RT ionic conductivity by up to two orders was observed in the corresponding Trilayer composites. We show that the high interfacial impedance of the surface polymer layers at the top/bottom surfaces of the composite membrane with the ceramic scaffold dominated the overall impedance. The Li^+ transference number (measured at 70 ºC) of scaffold-based Trilayer CPE ("Trilayer CPE w/ Porous Scaffold"), however, was still improved compared to the crosslinked-PEO+LiTFSI polymer electrolyte (0.29 vs. 0.05). As a result, the this composite

showed flatter overpotentials during Li//Li symmetric cell cycling and faster equilibration of potential gradients during cell relaxation between strip/plate steps compared to a pure crosslinked-PEO+LiTFSI membrane, implying formation of lower concentration gradients and confirming the utilization of ceramic phase for ion transport within the bulk of the composite. These comprehensive characterizations of the scaffold as well as the resulting CPEs provide an in-depth understanding of the role of ceramic scaffold's architecture, and polymer/ceramic interfaces on their electrochemical properties.

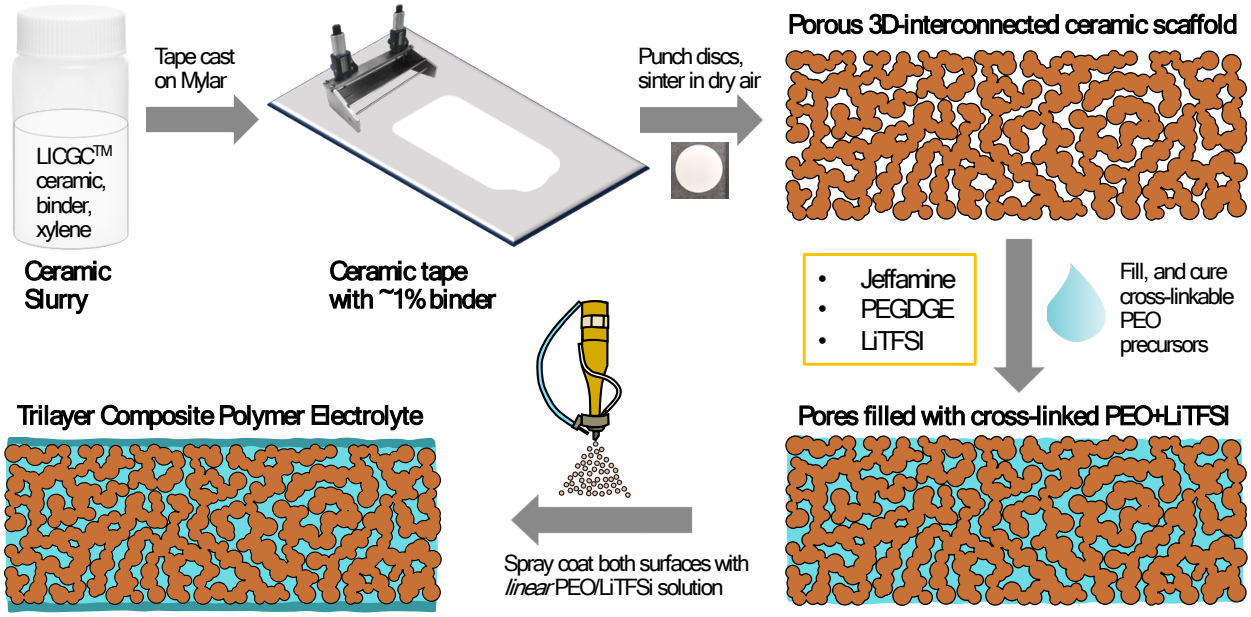

Scheme 1. Schematic representation of the fabrication process of Trilayer with Porous LICGC™ Scaffold.

Experimental methods

Fabrication of ceramic green tape

Free standing LICGC™ green tapes were fabricated using a tape casting process. Slurries of LICGC™ powder (1 µm, Ohara Corporation) were made by mixing it with binder (MSB1-13 from Polymer Innovations, Inc.) and xylene solvent using a standard roll jack/ball mill approach. ~ 175 µm thick tapes were cast on a Mistler tape caster. The "low-solids" slurry consisted of 38.9 wt% LICGC™, 0.5 wt.% binder, and 60.6 wt.% xylene (ceramic/binder=98.7:1.3 w/o solvent). The "high-solids" slurry consisted of 49.6 wt.% LICGC™, 0.5 wt.% binder, and 49.9 wt.% xylene (ceramic/binder=99:1 w/o solvent).

Fabrication of 3D composite membrane

The green tape was punched into 5/8" diameter discs which were sintered in dry air using various sintering profiles (**Table S1**) to obtain 3D-interconnected porous LICGC™ scaffolds. These were then infiltrated with cross-linkable polymer electrolyte precursor solution. To prepare the polymer precursor solution, 0.64 g of Jeffamine ED2003 (Eastman) and 0.35 g of LiTFSI (3M) were mixed with 0.60 g of ethanol (Sigma-Aldrich) in a glass vial and stirred at RT until a clear solution was

obtained (~30 min). The vial was then placed in a vacuum oven at RT overnight to evaporate off the ethanol. Next day, 0.32 g of poly(ethylene glycol) diglycidyl ether (PEGDGE 500, Mn 500, Sigma-Aldrich) was added to the glass vial and stirred for ~1 h to obtain a viscous precursor solution. Chemical structures of the precursor molecules are shown in **Figure S1**. Based on the volume % of porosity in the ceramic scaffold disc and density of the crosslinked-PEO+LiTFSI polymer (1.4 g/cm^3), amount of precursor solution needed per sample for 100% infiltration was calculated. Approximately 5-10% less of this calculated amount was dropped onto one side of the scaffold disc (to ensure no excess surface polymer layer was present on both surfaces), and the sample was left covered overnight at RT to allow the solution to completely infiltrate. Next day, the sample was transferred to an oven at 100 °C to thermally cure the liquid precursors. After about ~4 h of curing, vacuum was turned on to let the sample dry at 50-60 °C over several days, after which the sample was transferred to a spray coater for depositing thin layers of linear-PEO+LiTFSI polymer electrolyte on the two surfaces of each sample disc. Note, even a day-old precursor solution left at RT will cure to some extent to cause significant thickening making it difficult to infiltrate.

Spray coating was performed using an automatic ultrasonic spraycoater (Prism-400 BT from Ultrasonic Systems, Inc.) The spray coating solution consisted of acetonitrile, PEO (M.W. 400,000, Sigma Aldrich) and LiTFSI, where the concentration of PEO was 0.5 wt.% and the weight ratio of PEO to LiTFSI was kept to 3:1. The solution was spray coated onto the infiltrated LICGC™ discs placed on an alumina substrate heated at 40°C. The ultrasonic feature was disabled to avoid polymer degradation. After the spray nozzle completed rastering the defined area once, the sample was allowed to dry for one minute. The spraying/drying process was repeated until the desired thickness (~5 μm) was reached. After overnight drying under vacuum at 100 ºC, the trilayer samples were transferred to an argon glove box. Similar spray coating process was applied to dense LICGC™ plates (Ohara Corporation) to obtain corresponding trilayer samples. The two types of trilayer samples are called as “Trilayer CPE w/ Porous Scaffold”, and “Trilayer CPE w/ Dense Ceramic” in the text and figures.

Pure cross-linked PEO+LiTFSI membrane was also prepared as control. Precursor solution was prepared in the same composition as above in addition with 1.31 g isopropanol, followed by casting and curing in aluminum dishes. Pure linear-PEO+LiTFSI (3:1 by wt.) control membrane was prepared by making a 5 wt.% solution in acetonitrile which was cast into a flat-bottom Teflon dish, followed by drying under ambient conditions. Secondary drying was performed in a vacuum oven at 50-60 ºC over several days before transferring to the argon glove box.

Characterization of composite membranes

To prepare samples for cross-section imaging under SEM, a piece of trilayer sample was cooled down to −120 °C in a nitrogen filled cryo-chamber (Leica EM FC7). After cooling down to the target temperature, the sample was fractured inside the chamber with a sharp razor blade cooled to the same temperature. The sample was allowed to gradually warm up to room temperature in the nitrogen environment before loading into the SEM sample chamber for imaging.

Electrochemical characterizations

Ionic conductivity of partially sintered LICGC™ scaffolds was measured by first sputtering a thin layer of Au on both surfaces using a house-made sputtering system, to create the blocking electrodes. The gold coated sample was then transferred into a glove box and placed in a clamp that was connected to a BioLogic (SP-240) channel coming into the glove box. AC impedance

spectra were measured from 7MHz to 100mHz with a voltage amplitude of 6 mV at RT. Spectra were analyzed using the "Z fit" tool within the EC-Lab® software. To obtain the ionic conductivity of other samples, CR2032 coin cells were assembled where the stainless-steel spacers acted as the blocking electrodes. To obtain temperature dependence of the ionic conductivity, cells were connected to a BioLogic (SP-300) and placed in an ESPEC SU-222 temperature-controlled chamber. Two heat/cool cycles from 20 °C to 80 °C were applied for each measurement, with AC impedance (7 MHz to 100 mHz at 6 mV amplitude) collected after 1 h of thermal equilibration at each 10 °C temperature increment. Ionic conductivities obtained during the second cool cycle are reported here. Heat/cool cycles allow all interfaces to get equilibrated. Because of the fragile nature of the unfilled ceramic scaffolds, their Arrhenius plots could not be measured in coin cells.

Li^+ transference number (t_+) was obtained using the Bruce and Vincent method.[23] Specifically, the electrolyte membranes were made into Li symmetric cells and were equilibrated at 70 °C for 48 hours. After equilibration, the impedance was measured at open circuit voltage (OCV) using an impedance spectrometer (Biologic VSP-300). Then chronoamperometric measurement was carried out at an applied potential (ΔV) of 10 mV for 10 hours. At the end of 10 hours' polarization time, the impedance was measured with the applied 10 mV potential. The cation transference number (t_+) was then calculated using **Equation 1**. The initial current (I_o) is calculated using Ohm's law $\Delta V = I_O . R_\Omega$, where ΔV = 10 mV is the applied bias, and R_Ω is the total cell resistance obtained from the impedance spectrum prior to applying DC bias. As the concentration gradient is established in the cell, the steady state current, I_{ss}, is read from the chronoamperometry at the end of 10 hours of equilibration. R_o is the initial interfacial resistance and R_{ss} is the steady state interfacial resistance.

$$\boldsymbol{t_+ = \frac{I_{ss}}{I_0}\left(\frac{\Delta V - I_0 R_0}{\Delta V - I_{ss} R_{ss}}\right)} \quad (1)$$

Li//Li symmetric cells were fabricated in CR2032 coin cell format. Two lithium electrodes used were from Albemarle Corporation (~40 µm thick). The diameter of one Li disc was larger than the other to ensure complete overlap of smaller lithium, the area of which was used to normalize the current densities. After conditioning the cells for at least one day at 70 °C in an ESPEC SU-222 chamber, the cells were cycled at 70 °C using a BioLogic (VSP-3e) potentiostat. For long-term cycling, 0.2 mA/cm^2 current was applied with each stripping/plating half cycle being 2.5 h long, resulting in the passage of 0.5 mAh/cm^2 capacity. 1 h long rest was applied between each strip/plate half cycle to allow the concentration gradients generated during cycling to dissipate. Cycling started with stripping from the smaller Li electrode on to the larger Li electrode. Rate capability was determined by cycling at different currents/times with 1 h rest in-between. Similar symmetric cells were utilized for linear sweep voltammetry (LSV) tests to determine limiting current densities, where the voltage was increased at 0.05 mV/s. Li//NMC622 full cells were also assembled with the trilayer CPE and the control cross-linked PEO+LiTFSI membranes as the electrolyte and separator. Dried cathode composition was 88.8 wt.% NMC622 (polycrystalline, MSE Supplies), 4.9 wt.% carbon black (SUPER C65 carbon, TIMCAL), 6.3 wt.% PEO + LiTFSI (3:1 by wt.). Theoretical NMC622 areal loading was ~0.7 mAh/cm^2 for an upper cut-off voltage of 4.2 V vs. Li/Li^+. All coatings were subsequently cold calendered to reduce the porosity. A linear-PEO+LiTFSI (3:1 by wt.) electrolyte membrane was inserted between the cathode and electrolyte layer in all cells to improve contact with the composite cathode, as well as to make the electrolyte/cathode interface consistent among the various test cells [24]. After assembly, cells

were conditioned at 70 ºC for 48 h, after which charge/discharge cycling was done at a constant current of 0.2 mA/cm^2 between 2.9-4.2 V, with 1 h rest between charge/discharge.

Results and discussion

Scheme 1 shows schematically the fabrication process of a typical Trilayer with Porous LICGC™ Scaffold. First, a slurry of 1 μm LICGC™ particles was prepared which was tape cast on to mylar foils. After the drying, the green tape was flexible and could be easily peeled off from the mylar substrate. Small discs were subsequently punched out from the green tape which were then sintered in dry air to obtain porous, partially sintered LICGC™ ceramic scaffold. Scaffolds of various porosities and ionic conductivities were prepared by varying the sintering conditions as well as the initial packing of ceramic particles in the green tape. (**Figure 1a, Table S1**). Porosity (in volume %) of the scaffolds was estimated based on their weight, dimensions, and the theoretical density of LICGC™ (3.05 g/cm^3), and ranged between 40-52 vol.%. Overall, higher sintering temperatures and longer sintering times led to reduced porosity and higher ionic conductivity. The initial packing of ceramic particles was varied by adjusting the composition of the slurry, and was found to also have significant impact on the porosity and ionic conductivity of the resulting scaffold, for a given sintering profile (**Table S1**). For example, partial sintering of a hydraulically pressed LICGC™ green pellet without any binders resulted in an ionic conductivity of 1.8 x 10^{-5} S/cm (45% porosity), compared to 2.6 x 10^{-6} S/cm (52% porosity) for a green tape made with 'low solids' slurry, and 1.2 x 10^{-5} S/cm (48% porosity) for a green tape made with 'high solids' slurry; all sintered at 1000 °C for 3h. Slurry details are available in the experimental section. The ceramic scaffolds obtained from the 'high solids' slurry (1.2 x 10^{-5} S/cm), 'low solids' slurry (2.6 x 10^{-6} S/cm), and the dense LICGC™ plate (2.9 x 10^{-4} S/cm) were selected for subsequent CPE preparation steps.

Figure 1a provides an opportunity to analyze the conductivity data with respect to the effective medium theories (EMT) and estimate the highest theoretical conductivity achievable in the scaffolds. The McLachlan Generalized EMT (GEMT) is often used to describe the effective properties of particulate composites with randomly dispersed phases.[25] The equation for the effective conductivity, σ_{eff} is

$$\frac{g\left(\sigma_f^{1/t}-\left(\sigma_{eff}\right)^{1/t}\right)}{\sigma_f^{1/t}+\left(\frac{1-g_e}{g_e}\right)\left(\sigma_{eff}\right)^{1/t}}+\frac{(1-g)\left(\sigma_m^{1/t}-\left(\sigma_{eff}\right)^{1/t}\right)}{\sigma_m^{1/t}+\left(\frac{1-g_e}{g_e}\right)\left(\sigma_{eff}\right)^{1/t}}=0 \qquad (2)$$

where g, and g_e are the volume fraction of the conductive particles (1 μm diameter) in the composite and the percolation threshold respectively, t is the percolation slope (taken to be 1.3), and σ_m is the conductivity of the "matrix", i.e. the material containing filler particles of conductivity σ_f . **Equation 2** was solved numerically for σ_{eff} using Newton's method and the results are shown together with the experimental values of the conductivity of the LICGC™ scaffold in **Figure 1b**. These are obtained for the percolation threshold of 0.5, i.e. loose random packing limit. The conductivity values are normalized with respect to the maximum achievable conductivity in fully dense LICGC™ plate which is equal to 2.9 x 10^{-4} S/cm (**Table S1**). The

conductivity of the empty space was taken four orders of magnitude smaller than this value (to perform numerical solution with sufficiently small value), and the arrows in **Figure 1b** indicate drop of the effective conductivity to zero. The measured conductivities of the scaffold fall nicely on the GEMT curve.

The nice match between theoretical GEMT calculation and the experimental data solidly demonstrates that around the porosity of 50 vol%, the conductivity of randomly packed interconnected ceramic network is very sensitive to small changes of porosity. Specifically, a porosity increase from 46% to 51% caused more than 1 order of magnitude decrease in the resulting ionic conductivity of the ceramic network. Furthermore, at this porosity value, the highest reasonable conductivity that can be achieved is approximately 1/10 of the dense plate's conductivity. This value is significantly lower than that of the dense ceramic plate. Since around 50% porosity may be necessary in order maintain the connectivity of the polymer phase to ensure good flexibility of the composite, limited ionic conductivity is one of the intrinsic weaknesses of such randomly oriented interconnected ceramic network.

In addition to the predictions for the percolation driven behavior in composites, we placed the predicted conductivity based on the parallel brick layer model (PBLM) in **Figure 1b** which provides the upper limit of conductivity achievable in the most favorable configuration – layers of LICGC™ parallel to the electric field. At volume fraction corresponding to the percolation threshold of particulate composite, the conductivity of brick layered structure is 1.39 x 10^{-4} S/cm. This is the ideal conductivity of the vertically aligned LICGC™ structure taking 48 % of the volume, which is approximately 50% of the dense plate's value and much higher than the randomly-oriented case. This highlights the role of tortuosity in affecting the ionic conductivity for a similar porosity.

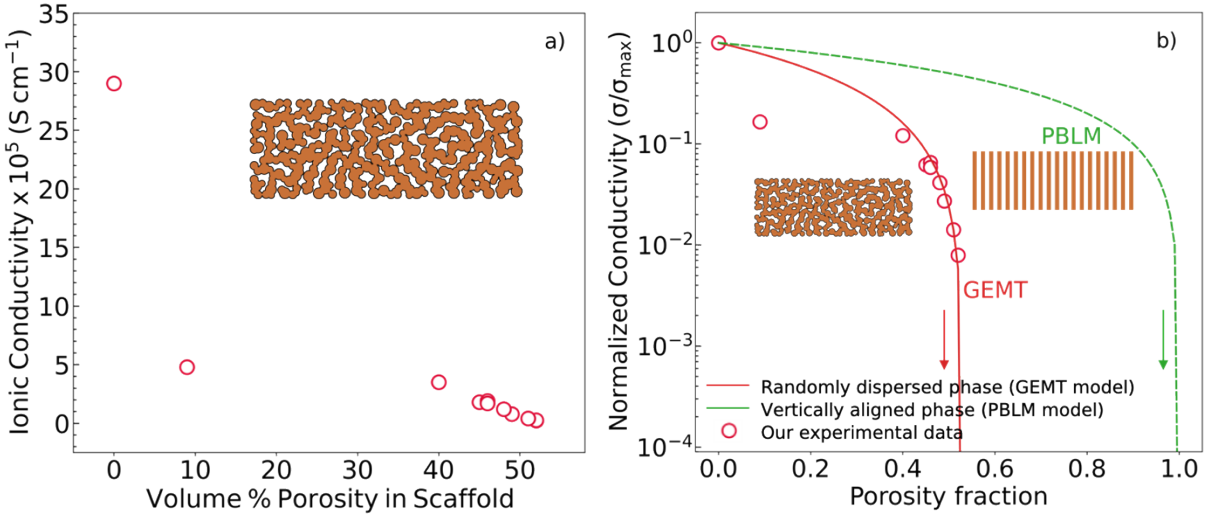

Figure 1. a) Ionic conductivity of the unfilled LICGC™ scaffolds as a function of volume % of their porosity. b) Ionic conductivity of the scaffolds compared to effective medium theory (EMT) calculations. The measured conductivities of the scaffold fall nicely on the GEMT curve, which predicts the conductivity of

randomly dispersed percolated particles. Conductivity of another morphology – vertically aligned percolated particles - is also modelled using PBLM model as a comparison.

The two porous scaffolds were infiltrated with a thermally cross-linkable polymer precursor solution (**Scheme 1**). Briefly, first Jeffamine ED2003 and LiTFSI were dissolved in ethanol until a clear solution obtained. The ethanol was dried off in a vacuum oven at RT overnight to get rid of the ethanol. Next day, PEGDGE500 was stirred in for an hour or so to obtain a viscous precursor solution which is completely solvent-free. This was important so that after curing there is no empty volume in the pores caused by loss of the solvent. The viscosity of this precursor solution is fortunately optimal such that it infiltrates but is not so thin that the gravity will bring a significant portion to the bottom. The amount of solution to be infiltrated was calculated based on the porosity of the disc to be infiltrated. Approximately 5-10% less of this calculated amount was dropped onto one side of the scaffold disc, as the addition of any excess solution caused it to remain on the top surface in the form of islands (not a uniform film). Based on the total weight after curing and initial scaffold porosity, the fraction of pores that were infiltrated was estimated to be ~90%. **Figure S2** shows surface images of the infiltrated scaffolds showing no excess surface layers. After letting the solution infiltrate at RT overnight, the sample was placed in an oven at 100 °C for complete curing. Next, thin layers (1-5 μm) of linear-PEO+LiTFSI electrolyte were spray coated on both surfaces of the infiltrated samples (**Scheme 1**). A full explanation of the reason for choosing crosslinked PEO to infiltrate and linear PEO to form surface layers is provided in the SI (page S-12). Spray coating of linear PEO+LiTFSI electrolyte was also performed on both sides of a dense LICGC™ plate. In total, three types of Trilayer CPEs were prepared with the ceramic scaffolds of 0%, 48%, and 52% porosity (labeled as Trilayer CPE w/ Dense Ceramic, Trilayer CPE w/ Porous Scaffold ("High Solids"), and Trilayer CPE w/ Porous Scaffold ("Low Solids")).

Figure 2a shows an SEM image of the surface of the green tape with uneven shaped ceramic particles with an average diameter of 1 μm. **Figures 2b** and **2c** show the ceramic tape cross-section after partial sintering. A 3D-interconnected scaffold containing uniform sized interconnected particles is typically observed after sintering. **Figures 2d-f** show the cross-section images of the Trilayer CPE w/ Porous Scaffold highlighting the middle, bottom surface, and top surface of the membrane. A complete infiltration of the LICGC™ scaffold with crosslinked-PEO+LiTFSI can be clearly seen in these images (cross-section EDS images in **Figure S2**). The linear-PEO+LiTFSI layers on the both surfaces are thin (<5 μm), unform, and well adhered to crosslinked-PEO+LiTFSI infiltrated ceramic middle layer. While the spray coater recipe aimed for a same thickness on both surfaces, the linear-PEO layer was for some reason found to be thicker on one side than the other (~3.2 μm and ~1.7 μm). This may be due to due to the precision range in volume control of the automatic spray-coater. Although for this study's purpose this was acceptable, as the main goal of the polymer layer was to, one, act as a barrier between LICGC™ ceramic and lithium metal electrode. Lithium readily reduces Ti^{4+} in the ceramic to result in an electronically conducting phase which leads to a self-propagating reduction reaction throughout the bulk of the interconnected membrane.[26, 27] Second, the soft linear-PEO+LiTFSI layer can form a conformal interface with the lithium metal anode. Third, the thin polymer layers also act as a proxy for excess polymer at the surface as a result of infiltration. Besides, PEO is known to be chemically stable with lithium metal.[28, 29] The cross-section images of Trilayer CPE w/ Dense Ceramic are

also shown in Figure 2g, h where the surface polymer layers can be seen as well-adhered to the ceramic middle layer.

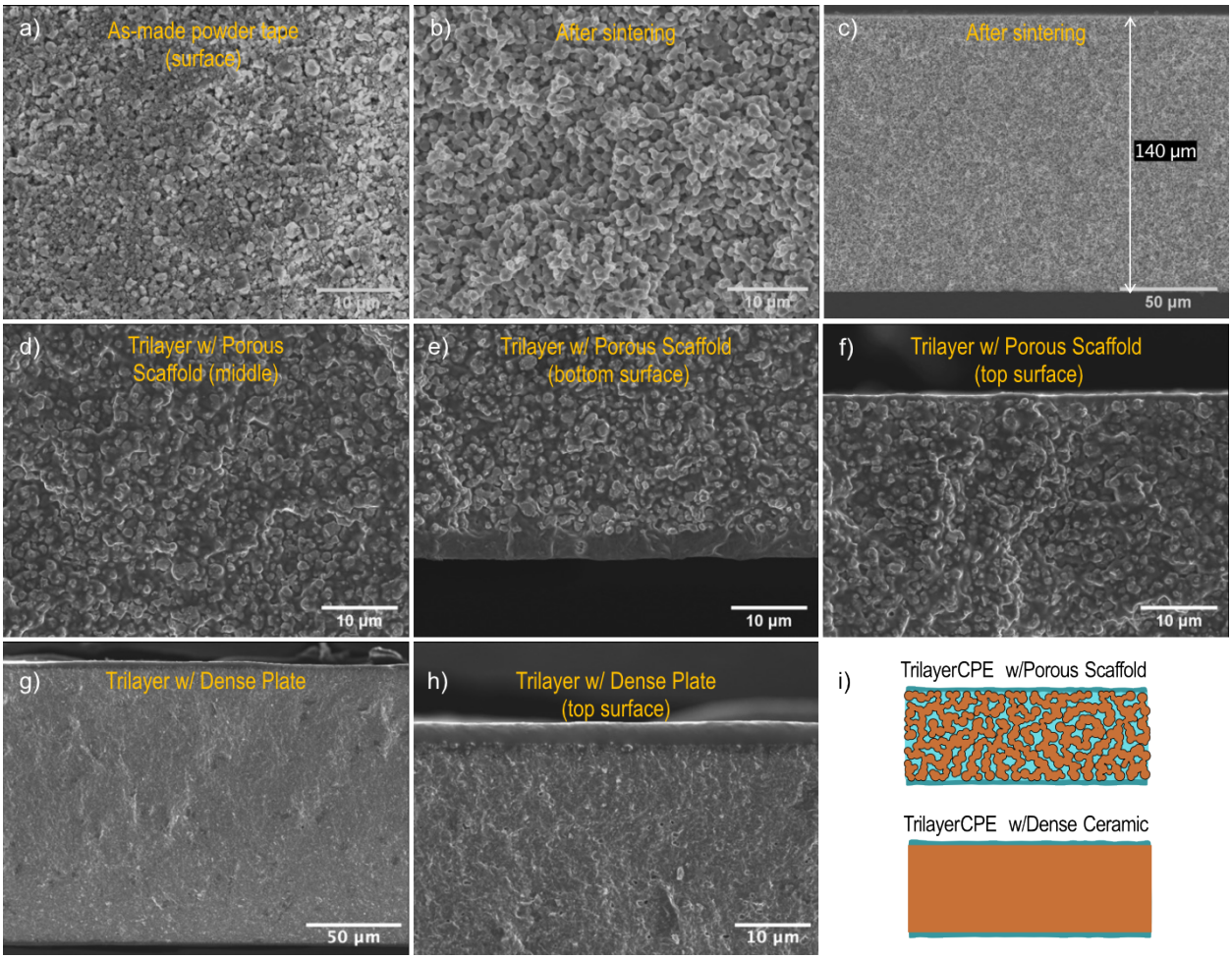

Figure 2. SEM images of a) surface of the as-cast green ceramic tape, b- c) cross-section of the sintered tape, d-f) cross-section of the sintered tape after filling with crosslinked-PEO+LiTFSI and spray coating the two surfaces with linear-PEO+LiTFSI ("Trilayer CPE w/ Porous Scaffold"), g, h) cross-section of the Trilayer CPE w/ Dense Ceramic. i) The two types of Trilayer CPEs shown schematically.

Figure 3a compares the Arrhenius plots of ionic conductivity of all three Trilayer CPEs along with the control cross-linked PEO-LiTFSI electrolyte. All Trilayer CPEs showed lower ionic conductivity than the cross-linked PEO+LiTFSI. When compared with the RT ionic conductivity of the corresponding ceramic scaffolds, a drop by up to 1-2 orders was observed (**Figure 3b**). For dense ceramic it dropped from 2.9 x 10^{-4} S/cm to 9.4 x 10^{-6}; for "high solids" porous scaffold, it fell from 1.2 x 10^{-5} S/cm to 2.6 x 10^{-6} S/cm; for "low solids" scaffold it dropped from 3.0 x 10^{-6} to 1.6 x 10^{-6} S/cm.

To understand the origin of this drop, EIS spectra were analyzed and compared. At low temperatures, two distinguishable semicircles before the tail were observed for all the Trilayer CPEs (**Figure S3**). A six-element equivalent circuit (R1 + Q2/R2 + Q3/R3 + Q4) was utilized, with two Q/R circuits corresponding to the two semicircles (**Figure S4**). The first semicircle (Q2/R2) has a capacitance of the order of 10^{-8} F, and the second semicircle has a capacitance of the order of 10^{-6} F (**Table S2**). We attributed the sum of first semicircle width (R2) and the x-axis

intercept (R1) to the bulk ionic conduction of the ceramic and polymer electrolyte phases. This attribution is consistent with impedance spectra of ceramic-only membranes and polymer-only membranes with blocking electrodes, that have capacitances in that range (**Figure S5**). The second semicircle (Q3/R3) is attributed to the polymer/ceramic interface (and the polymer/polymer interface between the two types of polymer electrolytes [30] for Trilayer CPEs w/ Porous Scaffolds), the only additional possible source of impedance (charge transfer impedance) in the trilayer samples. For the Trilayer w/ Dense Ceramic, this interface is only located at the top/bottom surface. For the Trilayer w/ Porous Scaffolds, the 3D-interconnected architecture of the ceramic and polymer phases likely allows parallel ion transport through each of those phases individually within the bulk of the membrane without crossing the high impedance polymer/ceramic interface of such high surface area, but the interface of infiltrated ceramic scaffold with the surface polymer layers will be unavoidable to cross.

We found that the resistance of between the bulk composite (or dense ceramic) and the surface polymer layer is much greater than total bulk impedance for all three Trilayer CPEs and dominates the overall impedance regardless of the ceramic phase's ionic conductivity (**Figure 3c**). Its absolute amount also scales with the total impedance of starting ceramic. As expected, infiltration of cross-linked PEO+LiTFSI electrolyte significantly reduced the bulk impedance compared to the bare ceramic scaffolds because of the replacement of air with an electrolyte of comparable ionic conductivity at RT (1.4×10^{-5} S/cm) that can allow conduction in parallel. Overall, the high impedance of interface with surface polymer dominated the overall impedance, and thus resulted in an order lower ionic conductivity compared to the bare ceramic scaffolds.

On the other hand, the transference number measured via Bruce and Vincent method was determined to be almost six times higher for the Trilayer CPE w/ Porous Scaffold ("high solids") (0.294), compared with the pure crosslinked-PEO+LiTFSI polymer electrolyte (0.054). **Figure 3d** shows the corresponding chronoamperometry curves normalized to the initial highest current. EIS spectra before/after polarization are available in **Figure S6**. A ceramic electrolyte has a transference number of nearly 1.0. Hence the current decay from the initial value in the chronoamperometry for Trilayer w/ Dense Ceramic is likely due to contributions from linear-PEO+LiTFSI phase and the resistive polymer/ceramic interface. For the Trilayer w/ Porous Scaffold ("high solids"), this likely also includes the contributions from cross-linked PEO+LiTFSI phase as it is one of the two ion transporting phases within the middle composite layer. However, the improvement in transference number compared to polymer electrolyte is attributed to the participation of ceramic scaffold in ion transport within the bulk of the composite. A control sample prepared with 50 wt.% LiCGC^{TM} ceramic particles dispersed within cross-linked

PEO+LiTFSI electrolyte showed little improvement in transference number compared to the pure polymer (**Figure S7**).

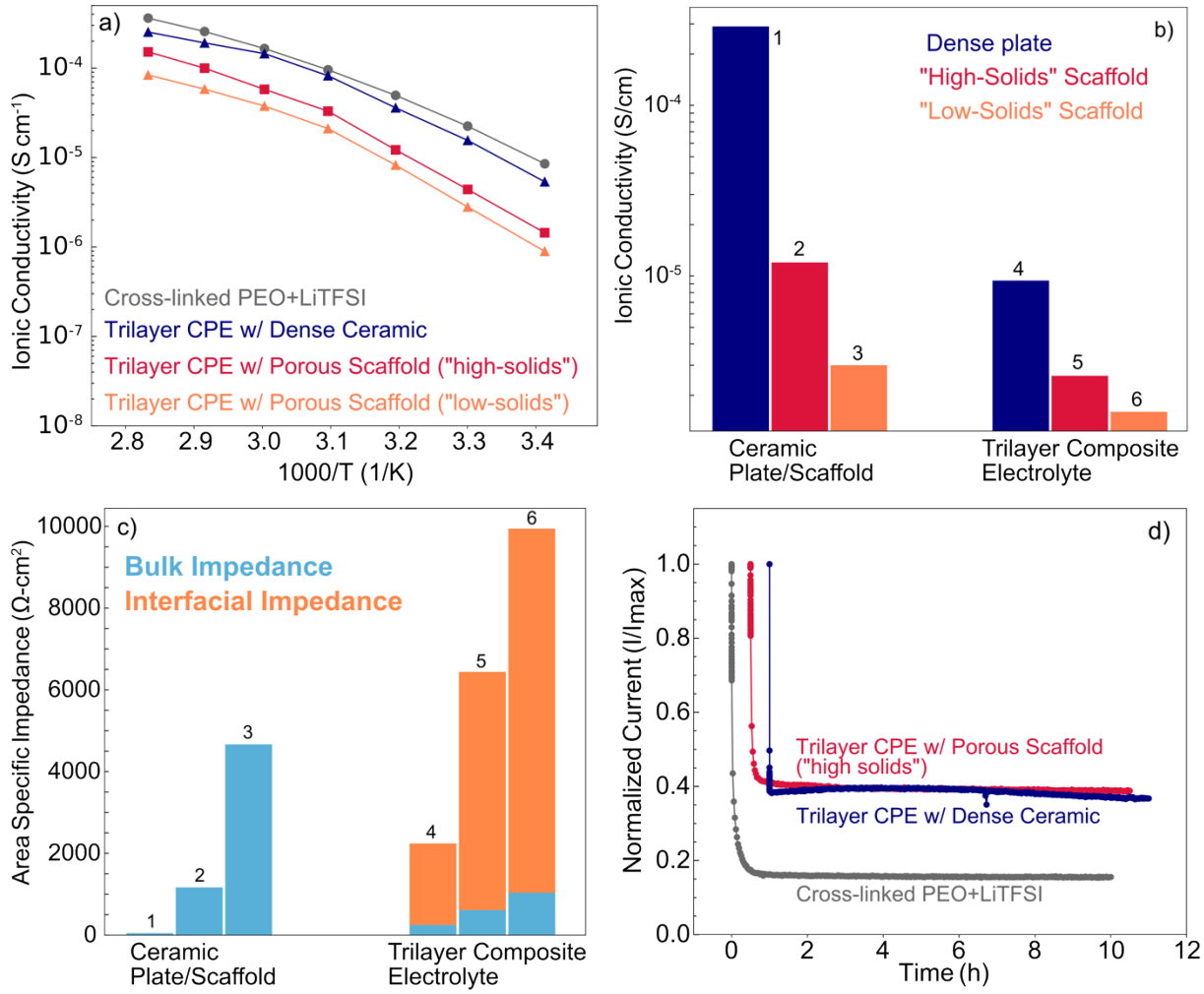

Figure 3. a) Arrhenius plot of the ionic conductivity of three types of Trilayer CPEs and the pure cross-linked PEO+LiTFSI. b) Bar chart comparing the RT ionic conductivities of the three types of bare ceramic scaffolds (dense ceramic, "high -solids" scaffold, and "low-solids" scaffold) with 0%, 48%, and 52% porosity, respectively, and their corresponding Trilayer CPEs. c) Bar chart comparing the area specific bulk and interfacial impedance of the six samples (numbered 1-6) show in b). d) Current v. time obtained during the chronoamperometry measurement, comparing the steady state current obtained after 10h of polarization, for the Trilayer CPE w/ Porous Scaffold ("high solids"), Trilayer CPE w/ Dense Ceramic, and the pure crosslinked-PEO+LiTFSI electrolyte.

A low transference number leads to generation of salt concentration gradients within dual-ion conducting electrolytes upon passage of current, and at high currents when the rate of diffusion cannot compensate for the rate of Li^+ consumption on the reducing electrode, a complete depletion of lithium salt can occur which are reflected in steep overpotentials during Li//Li symmetric cell cycling.[31-33] Indeed, because of the higher transference number of the Trilayer CPE w/ Porous Scaffold ("high solids"), flatter overpotentials are observed during cycling of the Li//Li symmetric cells compared to that of a pure crosslinked-PEO+LiTFSI membrane of similar thickness (**Figure 4a**), at currents up to 0.2 mA/cm^2. At higher currents, the polymer electrolyte and the Trilayer CPE

w/ Porous Scaffold ("high solids") both presented steep overpotentials. The Trilayer CPE w/ Dense Ceramic had the flattest overpotentials at 0.2 mA/cm^2 and was able to maintain flat potentials at higher currents, although the cell shorted and dendrite growth, which was unimpeded by the linear PEO+LiTSFI surface layer, severely fractured dense middle layer (**Figure S8**) . Interestingly, this is despite similar current decay to Trilayer CPE w/Porous Scaffold during chronoamperometry (**Figure 3d**), which means chronoamperometry may not be a good indicator of the flatness of voltage during galvanostatic cycling for this type of Trilayer CPE with a dense ceramic in the middle that comprises >95% vol% of the CPE. An in-depth understanding of this is beyond the scope of this work. In addition to overpotentials during cycling, the rate at which the cell voltage relaxes during rest step of these symmetric cells further highlights these differences of ion transport pathways and gradient formations within the various electrolytes (**Figure 4b**). The Trilayer CPE w/ Dense Ceramic instantly relaxes to zero volts, as the majority of ion conducting phase is 100% ceramic with unity transference number. The pure crosslinked-PEO+LiTFSI membrane relaxes the slowest as it is a complete dual-ion conductor with transference number of 0.05. The Trilayer w/ Porous Scaffold ("high solids") has an in-between rate of relaxation which suggests the participation of both ceramic and polymer phases for ion transport within the bulk of the electrolyte. The limiting current density (normalized for a 150 μm electrolyte thickness) measured via LSV at 0.05 mV/s was found to be similar (around 0.25 mA/cm^2) for both the pure polymer electrolyte and the Trilayer CPE w/ Porous Scaffold ("high solids") (**Figure 4c**). This is consistent with the results in **Figure 4a**. Li//NMC622 cells made with Trilayer CPE w/ Porous Scaffold ("high solids") also demonstrated higher charge/discharge capacities (~85% of theoretical capacity of 0.7 mAh/cm^2), compared to ~50% for the cell made with pure crosslinked-PEO+LiTFSI membrane, when cycled at 0.2 mA/cm^2. This is due to flatter and lower overpotentials allowed by the Trilayer CPE during galvanostatic cycling. Interestingly the rate of capacity decay is very different between the two cells. This cannot be answered with one single explanation because of the multiple inter-related factors at play in a full battery, and will be explored in a subsequent work. We also compared the high voltage oxidative stability of the two electrolytes, which was found to be similar (**Figure S9**). In terms of long-term Li//Li cycling, the Trilayer CPE w/ Dense Ceramic developed soft-shorts from cycle 5 onwards and led to unstable overpotentials and a hard short eventually (**Figure 4e**). This may be due the cycling-induced fracturing and reduction of the dense ceramic plate, as observed with the Li//Li cell in **Figure 4a** (photograph in **Figure S8**). Both the Trilayer CPE w/ Porous Scaffold, and the pure crosslinked-PEO+LiTFSI membrane are stable towards any dendrite formation for at least 700-800 h when cycled at 0.2 mA/cm^2 for 2.5 h each half-cycle in a Li//Li cell configuration. For the scaffold-based CPE, this suggests participation of ceramic in improving the transport properties without suffering from reduction and fracturing, as observed with the dense ceramic based trilayer CPE.

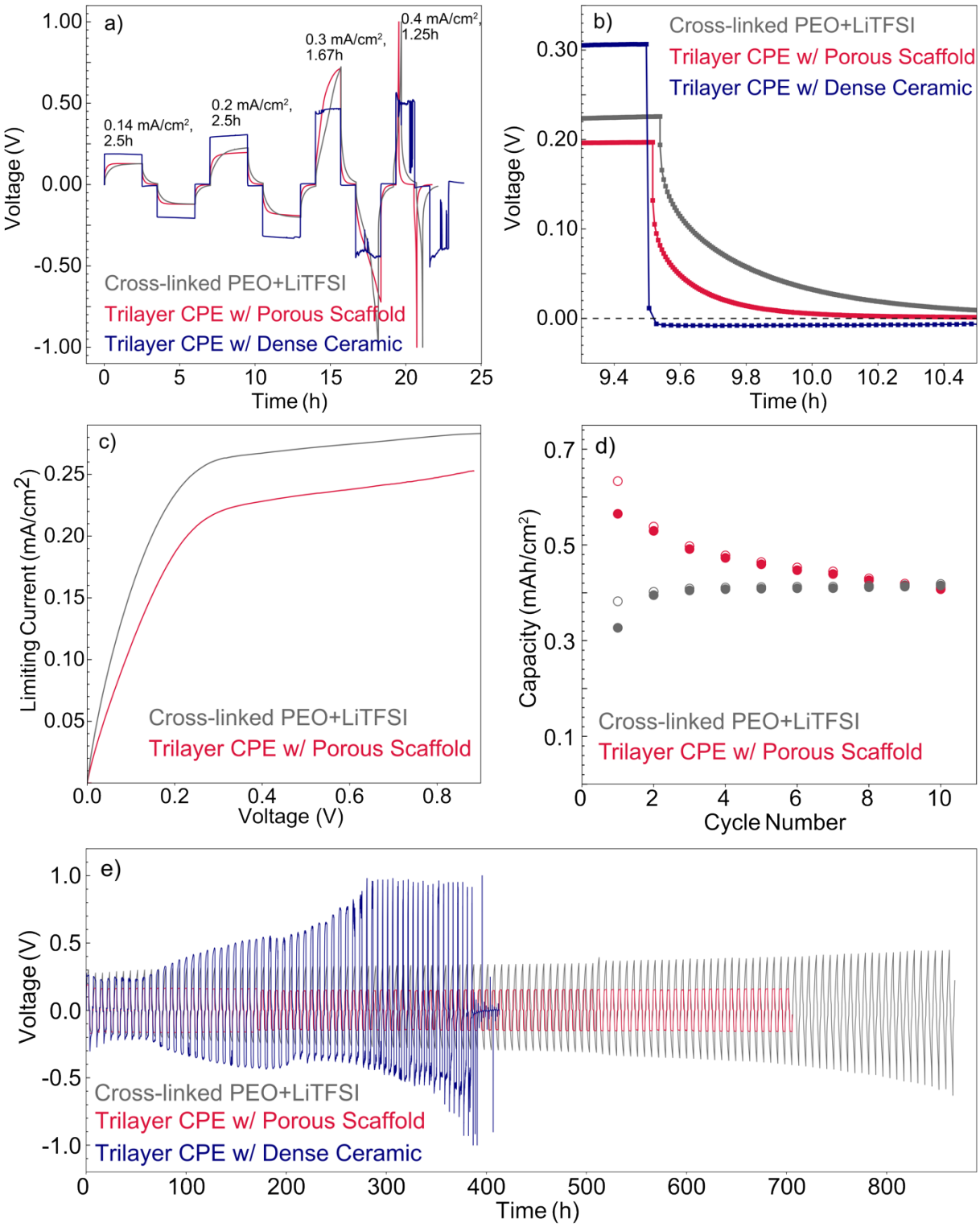

Figure 4. a) Voltage profiles of Li//Li symmetric cells made with Trilayer CPE w/ Porous Scaffold ("high solids"), Trilayer CPE w/ Dense Ceramic, and crosslinked-PEO+LiTFSI electrolytes, cycled at various current densities, at 70 ºC. b) Zoomed-in voltage profile observed during the 1 h

rest step after the second half cycle of the three cells shown a). c) Current density - voltage curves obtained via linear sweep voltammetry with a scan rate of 0.05 mV s^{-1}. d) Li//NMC622 cycling at 0.2 mA/cm^2 and 70 °C, with charge capacities shown as hollow circles and discharge capacities as filled circles. e) Long-term cycling of Li//Li symmetric cells at 0.2 mA/cm^2, 2.5 h each strip/plate, and 70 °C.

We also compare our results with other composite electrolytes reported in the literature that share similarities with this work in terms of the use of an interconnected ceramic framework and/or high ceramic volume fraction (>40-50 vol. %) in the composite electrolyte design (**Table 1**). Similar to this work, all these examples did not have any plasticizers (as reported) and have polymer layers covering the surface either applied as an extra step or as a result of infiltration/mixing. Majority of the CPEs with interconnected ceramic scaffolds did not report the ionic conductivity of the starting scaffold itself, and all but two did not report information on the transference number or limiting current densities. Consistencies and discrepancies between our results and literature can be noticed. Our results bear the most similarity with Ref 18 and 34 in terms of a similar total ceramic volume fraction and composite electrolyte design. The ionic conductivity of the CPE reported in these two papers is similar to our results. The role of interfacial resistance was not studied in depth in these reports. Our work provides details of the impact of surface polymer layer and the resulting interfacial impedance on the performance of CPEs with similar designs.

Majority of the CPEs with interconnected ceramic scaffold had significantly higher ionic conductivities (0.9-2.5 x 10^{-4} S/cm) while having much lower (5-28 vol.%) total ceramic volume fractions [14, 15, 16, 17, 20], compared to our work and Ref 18 and 34. Excluding the effect of tortuosity, such low ceramic volume fractions should limit the ionic conductivity of the ceramic phase to maximum 5-28% of the dense ceramic's value, and even lower if the tortuosity is considered. This suggests the improvements to be majorly from the polymer phase or the polymer/ceramic interphase. Ref 19 had a high ceramic volume fraction of 46 % with a comparable ionic conductivity of the starting interconnected scaffold as ours, but again had a much higher ionic conductivity of the corresponding CPE, maybe because a different processing route (in situ polymerization on lithium) was used. Composite electrolytes with simply dispersed ceramic particles in high volume fractions yielded similar (ref 33) or higher (ref 35) ionic conductivities to ours. Notably, majority of these studies focus on the synthesis/design and performance of the CPE and did not report thorough electrochemical characterizations such as, analysis of EIS spectra, transference number and limiting current measurements, ionic conductivity of the scaffold itself. This renders any deeper comparison of this work's results with literature to explain the possible sources of these discrepancies not possible.

Table 1. A summary of the composition and electrochemical properties of composite electrolytes in literature using an interconnected ceramic framework and/or containing a high volume fraction of ceramic electrolytes. A "-" means that value was not provided in the paper.

Ceramic	σ @RT of CPE (S/cm)	Ceramic vol%	σ @RT of ceramic framework (S/cm)	CPE thickness (μm)	Surface polymer layer (?)	Surface layer thickness (μm)	t_+ of CPE	t_+ of PE	Ref
doped LATP (Trilayer w/ Porous Scaffold)	2.6 x 10^{-6}	52	1.2 x 10^{-5}	150	Yes	5	0.29	0.05	This work

doped LATP (Trilayer w/ Dense Ceramic)	9.4 x 10^{-6}	97	2.9 x 10^{-4}	145	Yes	5	Not applicable	0.1	This work
$Li_{1+x}Al_xTi_{2-x}(PO_4)_3$ (LATP, interconnected, ice templated vertically aligned pillars)	6.8 x 10^{-6}	40	-	100	Yes	-	-	-	[18]
$Li_{1.5}Al_{0.5}Ge_{1.5}(PO_4)_3$ (LAGP, densely compressed particles)	1 x 10^{-6}	87	Not applicable	-	Yes (thin conformal, particles visible at surface)	-	-	-	[34]
$Li_{1.4}Al_{0.4}Ti_{1.6}(PO_4)_3$ (LATP) (PEO-LATP dense plate-PEO trilayer)	2 x 10^{-6}	78	1.6 x 10^{-4}	640	Yes	70	-	-	[35]
$Li_{1.5}Al_{0.5}Ge_{1.5}(PO_4)_3$ (LAGP, dispersed particles)	2.0 x 10^{-5}	59	Not applicable	40-60	Yes	-	-		[36]
$Li_{1.3}Al_{0.3}Ti_{1.7}(PO_4)_3$ (3D interconnected, in situ polymerization)	2.0 x 10^{-4}	46	2.6 x 10^{-5}	260	-	-	0.48	0.12	[19]
LLZO electrospun fiber mat	2.5 x 10^{-4}	5-7	-	40-50	Yes	-	-	-	[16]
LLZO (bacteria cellulose templated fiber mat)	1.1 x 10^{-4}	14	-	70-100	Yes (thin conformal, particles visible at surface)	-	-	-	[20]
LLTO (sol-gel synthesis 3D interconnected)	8.8 x 10^{-5}	16	-	-	Yes (thin conformal, particles visible at surface)	-	-	-	[14]
LLZO (sol-gel synthesis 3D interconnected)	8.5 x 10^{-5}	28	-	150	Yes (thin conformal, particles visible at surface)	-	-	-	[15]
LLTO (electrospun fiber mat)	1.6 x 10^{-4}	9.4	-	130	Yes	15, 25	0.48	0.18	[17]

Conclusions

In summary, various 3D-interconnected ceramic/polymer composite electrolytes with well-controlled architecture were prepared, with the goal of systematically understanding the role of scaffold architecture and the presence of surface polymer layers on their electrochemical properties. Before introducing the polymer electrolytes, the scaffold architecture strongly dictates its ionic conductivity. For a randomly interconnected ceramic framework in 3D space, at a porosity of around 50%, the conductivity of the scaffold is very sensitive to the volume fraction of voids, and its maximum conductivity is approximately 1/10 that of the dense plate. Since around 50% porosity may be necessary for the scaffold to maintain connectivity of both the ceramic and the polymer phases, limited ionic conductivity is one of the intrinsic weaknesses of such randomly oriented interconnected ceramic framework. Possible solution to this bottleneck includes making an aligned ceramic framework.

After making the composite with polymer electrolytes, the interconnected ceramic framework avoids the high interfacial impedance at the polymer/ceramic electrolyte interface within the bulk of the composite electrolyte. However, the high impedance of such an interface with surface polymer layers present at the top/bottom surfaces of the composite membrane dominates the overall impedance regardless of the ceramic phase's ionic conductivity, resulting in 1-2 orders of drop in RT ionic conductivity compared to the bare ceramic. Compared to literature results, much higher ionic conductivities have been reported using interconnected fiber networks with much lower volume fractions of ceramic (5-28 vol%). In depth analysis of the interfacial ion transport of such designs in cross-comparison with our system is needed to understand and provide guidance of how to minimize the interfacial impedance in CPEs.

Finally, an improvement in transference number is observed for the porous scaffold-based trilayer composite (0.29 vs. 0.05) compared to the pure polymer electrolyte used, resulting from the participation of the ceramic phase towards ion transport. The interconnected scaffold-based composite also demonstrates superior tolerance to shorting and fracture as compared to a 100% dense ceramic based composite. In this sense, the interconnected composite design has significant potential should the above-mentioned drawbacks be solved. The comprehensive characterizations reported in this work provides important insights to guide future research directions towards scalable manufacturing of composite electrolytes with optimized architecture and interfaces.

Acknowledgements

This research was sponsored by the U.S. Department of Energy (DOE), Office of Energy Efficiency and Renewable Energy for the Vehicle Technologies Office's Advanced Battery Materials Research Program (Simon Thompson, Program Manager). The SEM in this work was performed and supported at the Center for Nanophase Materials Sciences in Oak Ridge National Lab, a DOE Office of Science user facility.

References

[1] M.J. Wang, E. Kazyak, N.P. Dasgupta, J. Sakamoto, Transitioning solid-state batteries from lab to market: Linking electro-chemo-mechanics with practical considerations, Joule 5(6) (2021) 1371-1390.

[2] P. Albertus, V. Anandan, C. Ban, N. Balsara, I. Belharouak, J. Buettner-Garrett, Z. Chen, C. Daniel, M. Doeff, N.J. Dudney, Challenges for and pathways toward Li-metal-based all-solid-state batteries, ACS Publications, 2021.

[3] M. Balaish, J.C. Gonzalez-Rosillo, K.J. Kim, Y. Zhu, Z.D. Hood, J.L. Rupp, Processing thin but robust electrolytes for solid-state batteries, Nature Energy 6(3) (2021) 227-239.

[4] S. Li, S.-Q. Zhang, L. Shen, Q. Liu, J.-B. Ma, W. Lv, Y.-B. He, Q.-H. Yang, Progress and Perspective of Ceramic/Polymer Composite Solid Electrolytes for Lithium Batteries, Advanced Science 7(5) (2020) 1903088.

[5] X.C. Chen, X. Liu, A. Samuthira Pandian, K. Lou, F.M. Delnick, N.J. Dudney, Determining and Minimizing Resistance for Ion Transport at the Polymer/Ceramic Electrolyte Interface, ACS Energy Letters 4(5) (2019) 1080-1085.
[6] F. Langer, M.S. Palagonia, I. Bardenhagen, J. Glenneberg, F. La Mantia, R. Kun, Impedance spectroscopy analysis of the lithium ion transport through the Li7La3Zr2O12/P (EO) 20Li interface, Journal of The Electrochemical Society 164(12) (2017) A2298.
[7] M. Keller, G.B. Appetecchi, G.-T. Kim, V. Sharova, M. Schneider, J. Schuhmacher, A. Roters, S. Passerini, Electrochemical performance of a solvent-free hybrid ceramic-polymer electrolyte based on Li7La3Zr2O12 in P (EO) 15LiTFSI, Journal of Power Sources 353 (2017) 287-297.
[8] F. Langer, I. Bardenhagen, J. Glenneberg, R. Kun, Microstructure and temperature dependent lithium ion transport of ceramic–polymer composite electrolyte for solid-state lithium ion batteries based on garnet-type Li7La3Zr2O12, Solid State Ionics 291 (2016) 8-13.
[9] M. Mehraj Ud Din, M. Häusler, S.M. Fischer, K. Ratzenböck, F.F. Chamasemani, I. Hanghofer, V. Henninge, R. Brunner, C. Slugovc, D. Rettenwander, Role of filler content and morphology in LLZO: PEO membranes, Frontiers in Energy Research (2021) 532.
[10] M. Weiss, F.J. Simon, M.R. Busche, T. Nakamura, D. Schröder, F.H. Richter, J. Janek, From liquid-to solid-state batteries: ion transfer kinetics of heteroionic interfaces, Electrochemical Energy Reviews 3(2) (2020) 221-238.
[11] D. Spencer Jolly, D.L.R. Melvin, I.D.R. Stephens, R.H. Brugge, S.D. Pu, J. Bu, Z. Ning, G.O. Hartley, P. Adamson, P.S. Grant, A. Aguadero, P.G. Bruce, Interfaces between Ceramic and Polymer Electrolytes: A Comparison of Oxide and Sulfide Solid Electrolytes for Hybrid Solid-State Batteries, Inorganics 10(5) (2022) 60.
[12] R. Sahore, Z. Du, X.C. Chen, W.B. Hawley, A.S. Westover, N.J. Dudney, Practical considerations for testing polymer electrolytes for high-energy solid-state batteries, ACS Energy Letters 6(6) (2021) 2240-2247.
[13] M.J. Palmer, S. Kalnaus, M.B. Dixit, A.S. Westover, K.B. Hatzell, N.J. Dudney, X.C. Chen, A three-dimensional interconnected polymer/ceramic composite as a thin film solid electrolyte, Energy Storage Materials 26 (2020) 242-249.
[14] J. Bae, Y. Li, J. Zhang, X. Zhou, F. Zhao, Y. Shi, J.B. Goodenough, G. Yu, A 3D nanostructured hydrogel ‐ framework ‐ derived high ‐ performance composite polymer lithium ‐ ion electrolyte, Angewandte Chemie International Edition 57(8) (2018) 2096-2100.
[15] J. Bae, Y. Li, F. Zhao, X. Zhou, Y. Ding, G. Yu, Designing 3D nanostructured garnet frameworks for enhancing ionic conductivity and flexibility in composite polymer electrolytes for lithium batteries, Energy Storage Materials 15 (2018) 46-52.
[16] K.K. Fu, Y. Gong, J. Dai, A. Gong, X. Han, Y. Yao, C. Wang, Y. Wang, Y. Chen, C. Yan, Y. Li, E.D. Wachsman, L. Hu, Flexible, solid-state, ion-conducting membrane with 3D garnet nanofiber networks for lithium batteries, Proc Natl Acad Sci U S A 113(26) (2016) 7094-9.
[17] K. Liu, R. Zhang, J. Sun, M. Wu, T. Zhao, Polyoxyethylene (PEO)| PEO–perovskite| PEO composite electrolyte for all-solid-state lithium metal batteries, ACS applied materials & interfaces 11(50) (2019) 46930-46937.
[18] H. Zhai, P. Xu, M. Ning, Q. Cheng, J. Mandal, Y. Yang, A flexible solid composite electrolyte with vertically aligned and connected ion-conducting nanoparticles for lithium batteries, Nano Letters 17(5) (2017) 3182-3187.

[19] Y. Yan, J. Ju, S. Dong, Y. Wang, L. Huang, L. Cui, F. Jiang, Q. Wang, Y. Zhang, G. Cui, In Situ Polymerization Permeated Three ‐ Dimensional Li+ ‐ Percolated Porous Oxide Ceramic Framework Boosting All Solid ‐ State Lithium Metal Battery, Advanced Science 8(9) (2021) 2003887.
[20] H. Xie, C. Yang, K. Fu, Y. Yao, F. Jiang, E. Hitz, B. Liu, S. Wang, L. Hu, Flexible, Scalable, and Highly Conductive Garnet-Polymer Solid Electrolyte Templated by Bacterial Cellulose, Advanced Energy Materials 8(18) (2018) 1703474.
[21] X. Zhang, J. Xie, F. Shi, D. Lin, Y. Liu, W. Liu, A. Pei, Y. Gong, H. Wang, K. Liu, Vertically aligned and continuous nanoscale ceramic–polymer interfaces in composite solid polymer electrolytes for enhanced ionic conductivity, Nano letters 18(6) (2018) 3829-3838.
[22] F. Wu, K. Zhang, Y. Liu, H. Gao, Y. Bai, X. Wang, C. Wu, Polymer electrolytes and interfaces toward solid-state batteries: Recent advances and prospects, Energy Storage Materials 33 (2020) 26-54.
[23] J. Evans, C.A. Vincent, P.G. Bruce, Electrochemical measurement of transference numbers in polymer electrolytes, Polymer 28(13) (1987) 2324-2328.
[24] R. Sahore, G. Yang, X.C. Chen, W.-Y. Tsai, J. Li, N.J. Dudney, A. Westover, A Bilayer Electrolyte Design to Enable High-Areal-Capacity Composite Cathodes in Polymer Electrolytes Based Solid-State Lithium Metal Batteries, ACS Applied Energy Materials 5(2) (2022) 1409-1413.
[25] D.S. McLachlan, M. Blaszkiewicz, R.E. Newnham, Electrical resistivity of composites, Journal of the American Ceramic Society 73(8) (1990) 2187-2203.
[26] P. Hartmann, T. Leichtweiss, M.R. Busche, M. Schneider, M. Reich, J. Sann, P. Adelhelm, J. Janek, Degradation of NASICON-type materials in contact with lithium metal: formation of mixed conducting interphases (MCI) on solid electrolytes, The Journal of Physical Chemistry C 117(41) (2013) 21064-21074.
[27] T. Zhang, N. Imanishi, S. Hasegawa, A. Hirano, J. Xie, Y. Takeda, O. Yamamoto, N. Sammes, Li ／ polymer electrolyte ／ water stable lithium-conducting glass ceramics composite for lithium–air secondary batteries with an aqueous electrolyte, Journal of The Electrochemical Society 155(12) (2008) A965.
[28] G. Appetecchi, S. Scaccia, S. Passerini, Investigation on the stability of the lithium ‐ polymer electrolyte interface, Journal of the Electrochemical Society 147(12) (2000) 4448.
[29] Y. Jiang, X. Yan, Z. Ma, P. Mei, W. Xiao, Q. You, Y. Zhang, Development of the PEO based solid polymer electrolytes for all-solid state lithium ion batteries, Polymers 10(11) (2018) 1237.
[30] C. Sångeland, T. Tjessem, J. Mindemark, D. Brandell, Overcoming the Obstacle of Polymer–Polymer Resistances in Double Layer Solid Polymer Electrolytes, The journal of physical chemistry letters 12(11) (2021) 2809-2814.
[31] L. Stolz, G. Homann, M. Winter, J. Kasnatscheew, The Sand equation and its enormous practical relevance for solid-state lithium metal batteries, Materials Today 44 (2021) 9-14.
[32] L. Stolz, S. Hochstädt, S. Röser, M.R. Hansen, M. Winter, J. Kasnatscheew, Single-ion versus dual-ion conducting electrolytes: The relevance of concentration polarization in solid-state batteries, ACS applied materials & interfaces 14(9) (2022) 11559-11566.
[33] Z.J. Hoffman, A.S. Ho, S. Chakraborty, N.P. Balsara, Limiting Current Density in Single-Ion-Conducting and Conventional Block Copolymer Electrolytes, Journal of the Electrochemical Society 169(4) (2022) 043502.

[34] C. Wang, Y. Yang, X. Liu, H. Zhong, H. Xu, Z. Xu, H. Shao, F. Ding, Suppression of Lithium Dendrite Formation by Using LAGP-PEO (LiTFSI) Composite Solid Electrolyte and Lithium Metal Anode Modified by PEO (LiTFSI) in All-Solid-State Lithium Batteries, ACS Applied Materials & Interfaces 9(15) (2017) 13694-13702.
[35] J. Liang, Q. Sun, Y. Zhao, Y. Sun, C. Wang, W. Li, M. Li, D. Wang, X. Li, Y. Liu, Stabilization of all-solid-state Li–S batteries with a polymer–ceramic sandwich electrolyte by atomic layer deposition, Journal of Materials Chemistry A 6(46) (2018) 23712-23719.
[36] Y.-C. Jung, S.-M. Lee, J.-H. Choi, S.S. Jang, D.-W. Kim, All solid-state lithium batteries assembled with hybrid solid electrolytes, Journal of The Electrochemical Society 162(4) (2015) A704.

ToC Figure and associated text

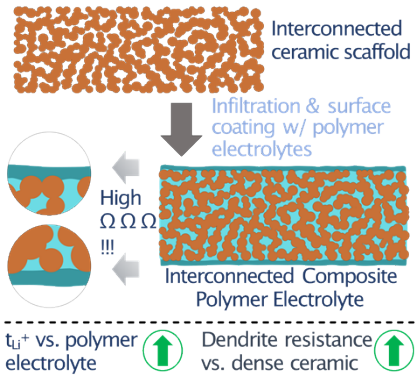

A three-dimensional interconnected ceramic/polymer composite electrolyte with a well-controlled architecture is fabricated and electrochemically investigated. Due to the bi-continuous ceramic and polymer phases, the composite presents improved transference number compared to neat polymer and improved dendrite resistance compared to dense ceramic. However, this work highlights the challenge that even with an interconnected framework, high impedance polymer/ceramic interface cannot be bypassed.